Received: 15 January 2019 | Revised: 3 April 2019 | Accepted: 15 April 2019

DOI: 10.1111/bph.14693

RESEARCH PAPER

Histidine at position 462 determines the low quinine sensitivity of ether-à-go-go channel superfamily member $K_v12.1$

Marlen Dierich[1] | Willem B. van Ham[2,3] | Anna Stary-Weinzinger[3] | Michael G. Leitner[1,4]

[1] Department of Neurophysiology, Institute of Physiology and Pathophysiology, Philipps-University Marburg, Marburg, Germany

[2] Department of Medical Physiology, University Medical Center Utrecht, Utrecht, The Netherlands

[3] Department of Pharmacology and Toxicology, University of Vienna, Vienna, Austria

[4] Division of Physiology, Department of Physiology and Medical Physics, Medical University of Innsbruck, Innsbruck, Austria

Correspondence
Michael G. Leitner, Division of Physiology, Department of Physiology and Medical Physics, Medical University of Innsbruck, Schöpfstraße 41, Innsbruck, Austria.
Email: michael.leitner@i-med.ac.at

Funding information
Deutsche Forschungsgemeinschaft, Grant/Award Number: LE 3600/1-1

Background and Purpose: The ether-à-go-go (Eag) K_v superfamily comprises closely related K_v10, K_v11, and K_v12 subunits. $K_v11.1$ (termed hERG in humans) gained much attention, as drug-induced inhibition of these channels is a frequent cause of sudden death in humans. The exclusive drug sensitivity of $K_v11.1$ can be explained by central drug-binding pockets that are absent in most other channels. Currently, it is unknown whether K_v12 channels are equipped with an analogous drug-binding pocket and whether drug-binding properties are conserved in all Eag superfamily members.

Experimental Approach: We analysed sensitivity of recombinant $K_v12.1$ channels to quinine, a substituted quinoline that blocks $K_v10.1$ and $K_v11.1$ at low micromolar concentrations.

Key Results: Quinine inhibited $K_v12.1$, but its affinity was 10-fold lower than for $K_v11.1$. Contrary to $K_v11.1$, quinine inhibited $K_v12.1$ in a largely voltage-independent manner and induced channel opening at more depolarised potentials. Low sensitivity of $K_v12.1$ and characteristics of quinine-dependent inhibition were determined by histidine 462, as site-directed mutagenesis of this residue into the homologous tyrosine of $K_v11.1$ conferred $K_v11.1$-like quinine block to $K_v12.1$(H462Y). Molecular modelling demonstrated that the low affinity of $K_v12.1$ was determined by only weak interactions of residues in the central cavity with quinine. In contrast, more favourable interactions can explain the higher quinine sensitivity of $K_v12.1$(H462Y) and $K_v11.1$ channels.

Conclusions and Implications: The quinoline-binding "motif" is not conserved within the Eag superfamily, although the overall architecture of these channels is apparently similar. Our findings highlight functional and pharmacological diversity in this group of evolutionary-conserved channels.

Abbreviations: Eag, ether-à-go-go channel; Elk, ether-à-go-go-gene-like channel; hERG, human ether-à-go-go-related gene channel 1; Erg, ether-à-go-go-related gene channel; LQT, long QT; MD, molecular dynamics; RMSD, root-mean-square deviation

1 | INTRODUCTION

The ether-à-go-go (Eag) superfamily of K_v channels comprises the three conserved families of Eag (K_v10), ether-à-go-go-related gene (Erg; K_v11), and ether-à-go-go-gene-like (Elk; K_v12) channels. These channels give rise to voltage-dependent K^+ currents in many cell types (Bauer & Schwarz, 2001; Bauer & Schwarz, 2018). The best characterised member, **K_v11.1** (termed **hERG** for the human isoform), engenders rapidly activating K^+ current I_{Kr} responsible for membrane repolarisation in cardiac myocytes (Sanguinetti, Jiang, Curran, & Keating, 1995). As I_{Kr} determines duration and end of heart action potentials, loss of K_v11.1 function constitutes a frequent cause of cardiac dysfunction in humans (Curran et al., 1995; Keating & Sanguinetti, 2001; Mitcheson, Chen, Lin, Culberson, & Sanguinetti, 2000; Sanguinetti et al., 1995; Trudeau, Warmke, Ganetzky, & Robertson, 1995). Mutations in **KCNH2**, the gene encoding K_v11.1, cause congenital long QT (LQT) syndrome-2 characterised by a prolonged QT interval and polymorphic ventricular arrhythmias (torsade de pointes) that may lead to recurrent syncope or sudden death (Curran et al., 1995; Sanguinetti et al., 1995). More common, however, are acquired forms of LQT syndrome through drug-induced inhibition of K_v11.1 (Keating & Sanguinetti, 2001; Roden, 1996; Sanguinetti et al., 1995). K_v11.1 channels are extremely sensitive to a wide variety of drugs including substituted quinolines (**quinidine**, **quinine**, and **chloroquine**), antiarrhythmic agents (e.g., MK-499 and dofetilide), and many other substances (e.g., terfenadine, cisapride, and vesnarinone; Furutani et al., 2011; Kamiya, Mitcheson, Yasui, Kodama, & Sanguinetti, 2001; Lees-Miller, Duan, Teng, & Duff, 2000; Mitcheson et al., 2000; Mitcheson et al., 2005; Sanchez-Chapula, Ferrer, Navarro-Polanco, & Sanguinetti, 2003; Sanchez-Chapula, Navarro-Polanco, Culberson, Chen, & Sanguinetti, 2002). All of these substances may cause undesired prolongation of cardiac action potentials by inhibiting K_v11.1 (Sanguinetti et al., 1995). The high susceptibility of human K_v11.1 to these structurally divergent drugs is governed by amino acids facing the channel's central cavity to form hydrophobic-binding pockets (Wang & MacKinnon, 2017). Mutagenesis studies have shown that amino acids in the inner pore helix (threonine 623), selectivity filter (serine 624 and valine 625), and tyrosine 652/phenylalanine 656 of the sixth transmembrane segment (S6) determine the susceptibility of drug-induced inhibition in K_v11.1 (Mitcheson et al., 2000; Sanchez-Chapula et al., 2002; Sanchez-Chapula et al., 2003; Wang & MacKinnon, 2017). Some of these residues are involved in drug binding (threonine 623, serine 624, tyrosine 652, and phenylalanine 656; Wang & MacKinnon, 2017), whereas others (e.g., valine 625 and also asparagine 588, serine 631, and serine 620) have been shown to control drug sensitivity through contributing to channel inactivation that is necessary for K_v11.1 inhibition through many high-affinity blockers (Ficker, Jarolimek, & Brown, 2001; Ficker, Jarolimek, Kiehn, Baumann, & Brown, 1998; Kamiya, Niwa, Mitcheson, & Sanguinetti, 2006; Perrin, Kuchel, Campbell, & Vandenberg, 2008; Wu, Gardner, & Sanguinetti, 2015). Further, phenylalanine 557 located in the S5 helix is involved in binding of some drugs (Helliwell et al., 2018; Saxena et al., 2016). Most of these residues are conserved in K_v10 channels, and accordingly, the **K_v10.1** isoform exhibits similarly high sensitivity to some substances (Schonherr, Gessner, Lober, & Heinemann, 2002). However, **K_v10.2** is significantly less susceptible to drug-induced inhibition, indicating that additional motifs might contribute to drug binding in certain members of the superfamily (Chen, Seebohm, & Sanguinetti, 2002; Gessner, Zacharias, Bechstedt, Schonherr, & Heinemann, 2004; Schonherr et al., 2002). In fact, it has been shown that high-affinity blockers of K_v11.1 are less effective on K_v10 channels, as these isoforms do not inactivate. This suggests that conformational reorientation of relevant residues associated with inactivation that are necessary for inhibition of K_v11.1 is absent in K_v10 channels (Chen et al., 2002; Ficker et al., 1998; Ficker et al., 2001).

In contrast to K_v10 and K_v11, only little information is available on the three members of the K_v12 (Elk) family predominantly expressed in neurons (Engeland, Neu, Ludwig, Roeper, & Pongs, 1998; Miyake, Mochizuki, Yokoi, Kohda, & Furuichi, 1999; Saganich, Machado, & Rudy, 2001; Shi et al., 1998; Trudeau, Titus, Branchaw, Ganetzky, & Robertson, 1999; Zou et al., 2003). **K_v12.2** regulates excitability of hippocampal neurons (Zhang et al., 2010), but no physiological role has been assigned to **K_v12.1** and **K_v12.3** channels yet. Recent studies provided significant insight into functional characteristics of K_v12.1 (Dai & Zagotta, 2017; Dierich, Evers, Wilke, & Leitner, 2018; Dierich & Leitner, 2018; Kazmierczak et al., 2013; Li et al., 2015), but it is unknown whether K_v12 channels are equipped with a high affinity drug-binding pocket as K_v10.1 and K_v11.1.

We analysed the sensitivity of human K_v12.1 to quinine, a substituted quinoline that blocks K_v11.1 channels at low micromolar concentrations (Gessner et al., 2004; Mitcheson et al., 2000; Sanchez-Chapula et al., 2003; Schonherr et al., 2002). Quinine also inhibited recombinant K_v12.1 channels, but their sensitivity was 10-fold lower than that of K_v11.1. Contrary to K_v11.1, quinine-dependent block of K_v12.1 was largely voltage-independent and the substance

What is already known

- Drug-induced inhibition of K_v11.1 (hERG) is a frequent cause of sudden death in humans.
- It is not known whether closely related K_v12 channels are also sensitive to drug-dependent inhibition.

What this study adds

- Low quinine sensitivity, affinity, and characteristics of inhibition of K_v12.1 channels are determined by H462.
- Drug sensitivity of K_v11.1 and K_v12.1 is different but determined by homologous amino acid positions.

What is the clinical significance

- Drug-binding pockets are not conserved in Eag superfamily members, but channel architecture is similar.
- Our findings facilitate the understanding of the arrhythmogenic actions of quinine.

induced channel opening at more depolarised membrane potentials. Mutagenesis of histidine at position 462 (H462) into the homologous tyrosine (Y652) of K_v11.1 conferred K_v11.1-like quinine sensitivity to K_v12.1(H462Y) channels. Molecular modelling analyses demonstrated that the low quinine sensitivity of K_v12.1 was determined by only weak interactions of quinine with H462 in the central cavity, whereas more favourable interactions facilitated higher quinine sensitivity of K_v12.1(H462Y) and closely related K_v11.1. Our data showed that the drug-binding pocket in the central cavity is not conserved in the Eag superfamily, although the general architecture of these channels is apparently similar. Our findings highlight functional and pharmacological diversity within this group of evolutionary conserved K^+ channels.

2 | METHODS

2.1 | Cell culture, transient transfection, and mutagenesis

CHO dhFR$^-$ cells (ATCC Cat# CRL-9096, RRID:CVCL_1977) were maintained as previously reported (Leitner et al., 2016). In brief, cells were maintained in MEM alpha medium (with 10% fetal calf serum and 1% pen/strep; all Invitrogen GmbH, Darmstadt, Germany) at 5% CO_2 and 37°C in a humidified atmosphere. Transient transfection of cultured CHO cells was performed using jetPEI (Polyplus Transfection, Illkirch, France). The following vectors for ion channel expression were used: K_v11.1 (Erg1)–pcDNA3.1 (gene: rat *Kcnh2*; UniProt accession number: O08962; UniProt, RRID:SCR_002380), K_v12.1 (Elk1)–pcDNA3.1–IRES–eGFP (human **KCNH8**; Q96L42), and pEGFP–C1 (transfection control; Addgene, Teddington, UK). An amino acid exchange (H462Y) was introduced into K_v12.1 with the QuikChangeII XL site-directed mutagenesis kit (Stratagene, Santa Clara, CA). Site-directed mutagenesis was confirmed by sequencing prior to the experiments (Microsynth SEQLAB, Göttingen, Germany).

2.2 | Electrophysiological recordings

Whole-cell patch clamp recordings were performed at room temperature (22–25°C) with an HEKA EPC10 USB patch clamp amplifier controlled by PatchMaster software (HEKA, Lambrecht, Germany; Patchmaster, RRID:SCR_000034). Voltage clamp recordings were low-pass filtered at 2 kHz and sampled at 5 kHz. The series resistance (R_s) was kept below 6 MΩ, and R_s was compensated throughout the recordings (80–90%; Dierich & Leitner, 2018; Leitner, Halaszovich, & Oliver, 2011). All voltage protocols are indicated in the figures; dashed lines highlight zero current. Borosilicate glass patch pipettes (Sutter Instrument Company, Novato, CA) had an open-pipette resistance of 2–3 MΩ after backfilling with intracellular solution containing (in mM) 135 KCl, 2.41 $CaCl_2$ (100-nM free Ca^{2+}), 3.5 $MgCl_2$, 5 HEPES, 5 EGTA, 2.5 Na_2ATP, and 0.1 Na_3GTP, pH 7.3 (with KOH), 290–295 mOsm·kg^{-1}. The extracellular solution contained (in mM) 144 NaCl, 5.8 KCl, 1.3 $CaCl_2$, 0.9 $MgCl_2$, 0.7 NaH_2PO_4, 10 HEPES, and 5.6 D-glucose, pH 7.4 (with NaOH), 305–310 mOsm·kg^{-1}. Liquid junction potentials were not compensated (approximately −4 mV).

2.3 | Analysis of electrophysiological recordings

Patch clamp recordings were analysed with IgorPro (Wavemetrics, Lake Oswego, OR; IGOR Pro, RRID:SCR_000325) and the PatchMaster (HEKA) software. Voltage-dependence of activation was derived from tail current amplitudes using voltage protocols indicated: Tail currents were fitted with a two-state Boltzmann function with $I = I_{min} + (I_{max} - I_{min})/(1 + \exp((V - V_h)/s))$, where I is the current, V is the membrane voltage, V_h is the voltage at half-maximal activation, and s describes the slope of the curve (s is presented as positive values to describe the slope of voltage-dependent channel activation; Leitner et al., 2012). Results are shown as conductance–voltage curves, obtained by normalising to ($I_{max} - I_{min}$), obtained from fits to data of individual experiments. For dose–response relationships, currents were normalised to baseline and were fitted to a Hill equation with $I = I_b + (I_{max} - I_b)/\left(1 + (IC_{50}/[S])^{n_H}\right)$, where I is the (normalised) current, I_b and I_{max} denote minimal and maximal currents, respectively, IC_{50} is the concentration at the half-maximal effect, [S] is the drug concentration, and n_H is the Hill coefficient. Time constants of activation were derived from mono-exponential fits to activating current components at indicated potentials (τ activation; c.f. Figure 3e). For presentation, whole-cell currents were normalised to cell capacitance (current density; pA·pF^{-1}) or to baseline current amplitudes (I/I_0; normalised current).

2.4 | Data and statistical analysis

The data and statistical analysis comply with the recommendations of the *British Journal of Pharmacology* on experimental design and analysis in pharmacology (Curtis et al., 2018). Isolated cells under investigation were randomly assigned to different treatment groups. Data analysis for experiments presented was performed in a blinded manner. For some experiments, single recordings were normalised to baseline values individually to account for baseline variations between cells. Statistical analysis was performed using Student's two-tailed t test/Wilcoxon–Mann–Whitney test, and when appropriate comparisons between multiple groups were performed with ANOVA followed by Dunnett's test. Post hoc tests were run only if F achieved $P < 0.05$ and there was no significant variance inhomogeneity. Significance was assigned at $P \leq 0.05$ ($^*P \leq 0.05$). Data subjected to statistical analysis have n over 5 per group, and data are presented as mean ± standard error of the means (SEM). In electrophysiological experiments, n represents the number of individual cells and accordingly the number of independent experiments (no pseudo-replication).

2.5 | Molecular modelling

A K_v12.1 homology model of the pore module (residues S352–Y477) in the open/inactive conformation was built using the programme modeller 9v.17 (Webb & Sali, 2016, RRID:SCR_008395) based on

the cryo-EM structure of the hERG (human $K_v11.1$) channel (pdb identifier: 5VA1, 3.7 Å resolution; Wang & MacKinnon, 2017). The sequence identity between target and template is 61% (sequence similarity: 76%). Docking studies were carried out with the Genetic Optimization for Ligand Docking program, version 5.6.2 (GOLD, Jones, Willett, Glen, Leach, & Taylor, 1997). The "chemscore" fitness scoring function was used, and all residues within 12 Å of residue H462 in $K_v12.1$ were defined as binding site. The Chemscore.DG scoring function was used to estimate free energies of binding. Side chains of residues H462 and F466 from all four domains were set as flexible. The pKa of H462 is calculated to be 3.13 (PROPKA; Olsson, Sondergaard, Rostkowski, & Jensen, 2011), indicating a hydrogen atom on the δ nitrogen. The other two tautomers were considered in docking as well; however, similar binding modes/poses were obtained. For molecular dynamics (MD) system setups and ligand parametrisation (Vanommeslaeghe et al., 2010), the CHARMM-GUI (Jo, Kim, Iyer, & Im, 2008; CHARMM, RRID:SCR_014892) was used. The quinine molecule was protonated at the tertiary N (pKa value of the quinolone group: 9.7, O'Neil, 2013). Protein–ligand complexes obtained from docking were embedded in a 1-palmitoyl-2-oleoyl-*sn*-glycero-3-phosphocholine bilayer and solvated with TIP3P waters. K^+ ions were placed in the selectivity filter at sites S0, S2, and S4, with water molecules at sites S1 and S3 and 0.15-M KCl added to the simulation box. Energy minimisation, 20-ns equilibration, and three independent 50-ns production runs (with initial atom velocities assigned independently and randomly) were performed using GROMACS v.5.1.2 (GROMACS, RRID:SCR_014565; Abraham et al., 2016) with the charmm36 force field for protein molecules (incorporating CMAP terms, Mackerell, Feig, & Brooks, 2004) and lipid molecules and salt ions (Best et al., 2012; Klauda et al., 2010; MacKerell et al., 1998). Electrostatics were modelled using particle mesh Ewald (Darden, York, & Pedersen, 1993), and LINCS was used to constrain covalent chemical bonds to hydrogens (Hess, Bekker, Berendsen, & Fraaije, 1997). Temperature was maintained at 310 K using velocity rescaling (V-rescale; Bussi, Donadio, & Parrinello, 2007), and semi-isotropic pressure coupling was accomplished using the Parrinello–Rahman barostat (Parrinello & Rahman, 1981). MD trajectories were analysed using VMD v.1.9.2 (VMD, RRID:SCR_001820; Humphrey, Dalke, & Schulten, 1996) and GROMACS.

2.6 | Materials

Quinine was purchased from Tocris Bioscience (Bristol, UK) and was diluted in extracellular solution to concentrations indicated in Section 3. Quinine was applied locally via a glass capillary through a custom-made application system.

2.7 | Nomenclature of targets and ligands

Key protein targets and ligands in this article are hyperlinked to corresponding entries in http://www.guidetopharmacology.org, the common portal for data from the IUPHAR/BPS Guide to PHARMACOLOGY (Harding et al., 2018), and are permanently archived in the Concise Guide to PHARMACOLOGY 2017/18 (Alexander et al., 2017).

3 | RESULTS

3.1 | Voltage-independent but mode shift-dependent inhibition of $K_v12.1$ channels through quinine at high concentrations

We started our pharmacological analyses by applying increasing concentrations of quinine to CHO cells transiently expressing human $K_v12.1$. When activating $K_v12.1$ with 600-ms voltage steps to 0 mV from a holding potential of −60 mV, quinine inhibited $K_v12.1$ channels with an IC_{50} of 0.97 mM and a Hill coefficient of 1.0 (Figure 1a). At a concentration close to the IC_{50} (1 mM), this inhibition developed within seconds and was partially reversible after removal of the drug (Figure S1a,b). After having established the quinine sensitivity of $K_v12.1$, we set out to characterise effects of the substance on voltage-dependent activation of the channels. Noteworthy, $K_v12.1$ channels exhibit a mode shift of activation (also termed pre-pulse facilitation or voltage-dependent potentiation; Dai & Zagotta, 2017; Dierich et al., 2018; Dierich & Leitner, 2018; Li et al., 2015), which designates stabilisation of the voltage-sensing domain in a "relaxed" open state after prolonged depolarisation of the membrane potential (Bezanilla, Taylor, & Fernandez, 1982; Villalba-Galea, Sandtner, Starace, & Bezanilla, 2008). Most prominently, mode shift manifests through a large shift of activation voltages to hyperpolarised potentials following membrane potential depolarisation (Dai & Zagotta, 2017; Dierich et al., 2018; Dierich & Leitner, 2018; Li et al., 2015). To induce mode shift, we applied conditioning potentials of −60 or 0 mV (200 ms) before a series of voltage steps to activate $K_v12.1$ (pulse potentials: −140 to +20 mV; 600 ms; Figure 1b,c; c.f. Dierich & Leitner, 2018; Dierich et al., 2018). Following the hyperpolarised conditioning potential (−60 mV), half-maximal voltage (V_h) and slope factor of $K_v12.1$ channel activation were −30.0 ± 2.0 mV and 14.9 ± 1.1 mV, respectively (n = 6; Figure 1d–f). When we applied the conditioning potential of 0 mV, V_h was −75.9 ± 1.7 mV and s was 10.6 ± 0.5 mV (n = 6; Figure 1d–f). Depolarised conditioning potentials thus induced a large (and significant) shift of the voltages of activation of $K_v12.1$ channels to hyperpolarised potentials by about −45 mV, representing their mode shift of activation (Dai & Zagotta, 2017; Dierich et al., 2018; Dierich & Leitner, 2018; Li et al., 2015). Application of quinine (1 mM) shifted the voltage dependence of $K_v12.1$ to depolarised voltages for both conditioning potentials. As this shift was more pronounced after the depolarised conditioning potential (0 mV; Figure 1d,e), the degree of mode shift was significantly attenuated to about −23 mV in the presence of the substance (Figure 1e). Application of quinine (1 mM) inhibited both steady-state currents and tail currents through $K_v12.1$ channels (Figure 1g,h). Following both conditioning potentials, quinine-induced inhibition of steady-state $K_v12.1$ currents was the same for all activating voltages (Figure 1i; n = 6; e.g., for conditioning potential −60 mV: not significant

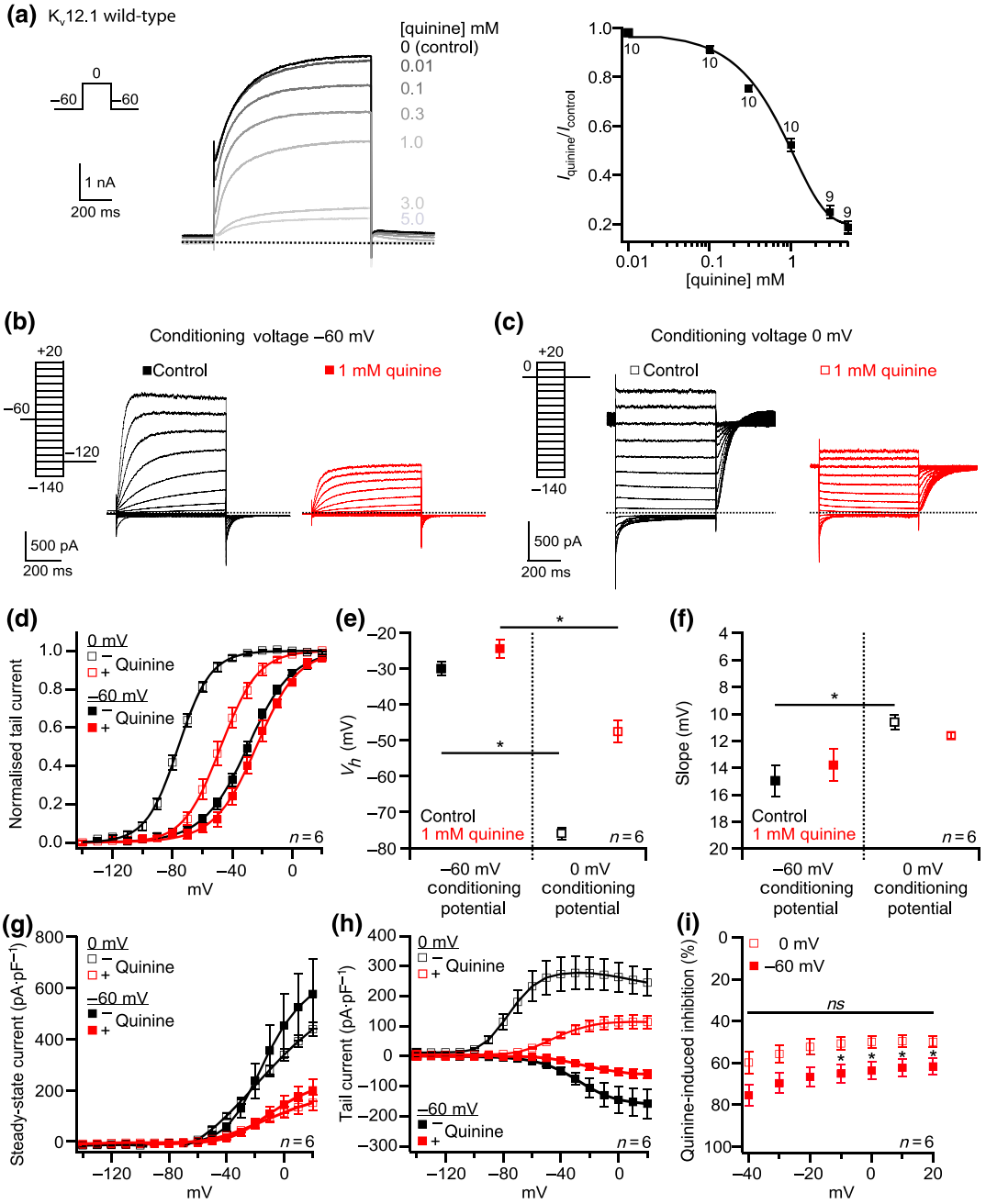

FIGURE 1 Quinine inhibits human $K_v12.1$ channels at high concentrations in a voltage-independent manner. (a) Dose-dependent inhibition of recombinant $K_v12.1$ channels through extracellular application of quinine. The panel shows representative recordings of a CHO cell expressing human $K_v12.1$ treated with increasing quinine concentrations (left) and the summarised quinine dose–response relationship (right; IC_{50} and Hill coefficient were calculated from a Hill fit to averaged recordings as shown in the left panel; solid line represents this fit). Scale bars, voltage protocol, quinine concentrations, and number of cells as indicated. (b–f) Quinine induced the activation of recombinant $K_v12.1$ channels at more positive membrane potentials. Representative recordings of $K_v12.1$ channels activated by voltage steps between −140 and +20 mV following 200-ms conditioning voltage steps to (b) −60 mV or (c) 0 mV before (control) and at the end of quinine application (1 mM). (d) Summary of voltage-dependence of $K_v12.1$ channels derived from Boltzmann fits to individual recordings as shown in (b, c); solid line represents Boltzmann fit to averaged data. (e) Mean V_h of channel activation and (f) summarised s factors of activation before and at the end of quinine treatment (1 mM; values derived from fits as shown in d). Quinine (1 mM) inhibited voltage-dependent (g) outward steady-state and (h) inward tail currents through recombinant $K_v12.1$ channels (current amplitudes analysed from recordings as shown in b, c). (i) Quinine-induced inhibition of $K_v12.1$ was voltage-independent (presented as % inhibition from data shown in (g); *ns*, no significant difference for quinine block between activating voltages of −40 and 20 mV). Note that quinine block was significantly more pronounced, when $K_v12.1$ channels were activated at membrane potentials more positive than −30 mV. *Significant difference of quinine block for both conditioning potentials

(*ns*) between −40 mV and +20 mV, $P = 0.54$), that is, quinine inhibited $K_v12.1$ channels in a voltage-independent manner. However, quinine-dependent block was significantly more pronounced following the hyperpolarised conditioning potential (−60 mV) for activating voltages more positive than −30 mV (indicated by "*" in Figure 1i). These data demonstrated that to some extent, $K_v12.1$ channels were more sensitive to quinine block after conditioning depolarisation of the membrane, and that accordingly, quinine block of $K_v12.1$ channels depended on mode shift.

3.2 | Quinine is a voltage- and mode shift-dependent inhibitor of $K_v11.1$ channels

We then compared our findings on $K_v12.1$ to quinine-dependent inhibition of closely related $K_v11.1$. In line with a previous study (Sanchez-Chapula et al., 2003), quinine inhibited recombinant $K_v11.1$ channels with an IC_{50} of 98 μM and a Hill coefficient of 1.3 (Figure 2a). Accordingly, the quinine affinity of $K_v11.1$ channels was about 10 times higher than that of $K_v12.1$ (c.f. Figure 1a). As for $K_v12.1$, quinine-dependent inhibition of $K_v11.1$ developed in seconds and was partially reversible (50-μM quinine; Figure S1c,d). By applying hyperpolarised (−60 mV) and depolarised (+40 mV) conditioning voltages before the activating pulse potentials, we then analysed effects of quinine on the voltage dependence of $K_v11.1$ channels that also exhibit mode shift of activation (Figure 2b,c). As previously reported (Dierich et al., 2018; Tan, Perry, Ng, Vandenberg, & Hill, 2012), depolarised conditioning potentials (+40 mV) significantly shifted the voltage dependence of $K_v11.1$ channels by about −50 mV compared with the hyperpolarised conditioning potential (Figure 2d–f). Following the hyperpolarised conditioning potential (−60 mV), quinine (50 μM) significantly shifted the voltage dependence of $K_v11.1$ channels by −13 mV to more negative potentials (Figure 2d–f). As the voltage dependence of $K_v11.1$ was not altered following the depolarised conditioning potential (+40 mV), the degree of mode shift was attenuated in the presence of quinine (50 μM; Figure 2d,e). Quinine blocked both voltage-dependent outward and inward currents through $K_v11.1$ (Figure 2g,h). After the conditioning potential of −60 mV, the degree of this inhibition was significantly increased, when the channels were activated at more positive potentials (Figure 2i), that is, quinine block was voltage dependent following the hyperpolarised conditioning potential. In contrast, following the depolarised conditioning potential, quinine block of $K_v11.1$ channels was completely voltage independent. Thus, for $K_v11.1$ channels, quinine-induced inhibition depended on mode shift (c.f. quinidine; Furutani et al., 2011), but (in contrast to $K_v12.1$) the $K_v11.1$ channels apparently were more sensitive to quinine following the depolarised conditioning potential, when activated at negative membrane potentials.

3.3 | Functional characterisation of $K_v12.1$(H462Y) channels

Sensitivity of human $K_v11.1$ channels to several drugs has been attributed to the amino acids T623, V625, Y652, and F656, located in the channels inner pore helix, selectivity filter, or sixth transmembrane segment (S6; Figure 3a; Lees-Miller et al., 2000; Mitcheson et al., 2000; Sanchez-Chapula et al., 2002; Sanchez-Chapula et al., 2003). As $K_v12.1$ also carries threonine, valine, and phenylalanine at homologous positions (T433, V435, and F466 in $K_v12.1$), we hypothesised that the amino acid exchange at position 462, where $K_v12.1$ has a histidine instead of the tyrosine (Figure 3a), determined the low quinine sensitivity of $K_v12.1$. To elaborate this hypothesis, we mutated H462 in $K_v12.1$ to the corresponding tyrosine (Y652) of $K_v11.1$ and characterised the $K_v12.1$(H462Y) mutant in CHO cells. Recombinant $K_v12.1$(H462Y) channels produced robust voltage-dependent and outwardly rectifying K^+ currents (Figure 3b,c). However, $K_v12.1$(H462Y)-mediated whole-cell currents were significantly smaller than for the wild-type channels (Figure 3b–d), and the mutant channels activated significantly faster than the wild-type, when activated through voltage steps between −40 and 0 mV (Figure 3e). For conditioning voltages of −60 and 0 mV, V_h was −38.0 ± 1.8 mV and −73.6 ± 1.6 mV, respectively, demonstrating that $K_v12.1$(H462Y) channels also exhibited a mode shift of activation (Figure 3f–h; $n = 9$). However, in the mutant, mode shift was attenuated compared with wild-type to about −35 mV (−45 mV in wild-type; c.f. Figure 1), mainly because $K_v12.1$(H462Y) activated at significantly more negative membrane potentials after the hyperpolarised conditioning potential of −60 mV (Figure 3f–h). The voltage dependence of wild-type and mutant channels was the same after the conditioning potential of 0 mV (Figure 3f–h).

3.4 | Histidine at position 462 determines the quinine sensitivity of human $K_v12.1$

When applying increasing quinine concentrations to CHO cells expressing $K_v12.1$(H462Y), we found that quinine inhibited this channel mutant with an IC_{50} of 56 μM and a Hill coefficient of 1.1 (Figure 4a). Thus, the quinine affinity of $K_v12.1$(H462Y) was about 17-fold higher than that of the wild-type channels and accordingly more similar to $K_v11.1$ (c.f. Figures 1a and 2a). As for $K_v12.1$ wild-type, application of quinine (50 μM) blocked inward and outward currents through $K_v12.1$(H462Y) (Figure 4b–e), but in contrast to the wild-type channels, quinine-mediated inhibition of $K_v12.1$(H462Y) was rapidly reversible (Figure S1e,f). Noteworthy, we detected a transient increase of currents in the presence of quinine, when activating $K_v12.1$(H462Y) at membrane voltages more positive than 0 mV (following the hyperpolarised conditioning potential; Figure 4b). This observation indicated that channel opening may be required for quinine-dependent inhibition of $K_v12.1$(H462Y). In line, quinine-induced inhibition of $K_v12.1$(H462Y) was more pronounced, when the channels where activated at more positive membrane voltages, that is, quinine block of $K_v12.1$(H462Y) was voltage dependent following positive and negative conditioning potentials (Figure 4f). For $K_v12.1$(H462Y) channels, this voltage dependence of quinine block presumably also caused a reduction of tail currents at depolarised activating voltages after conditioning potential of 0 mV (Figure 4e,g). Of special note, in

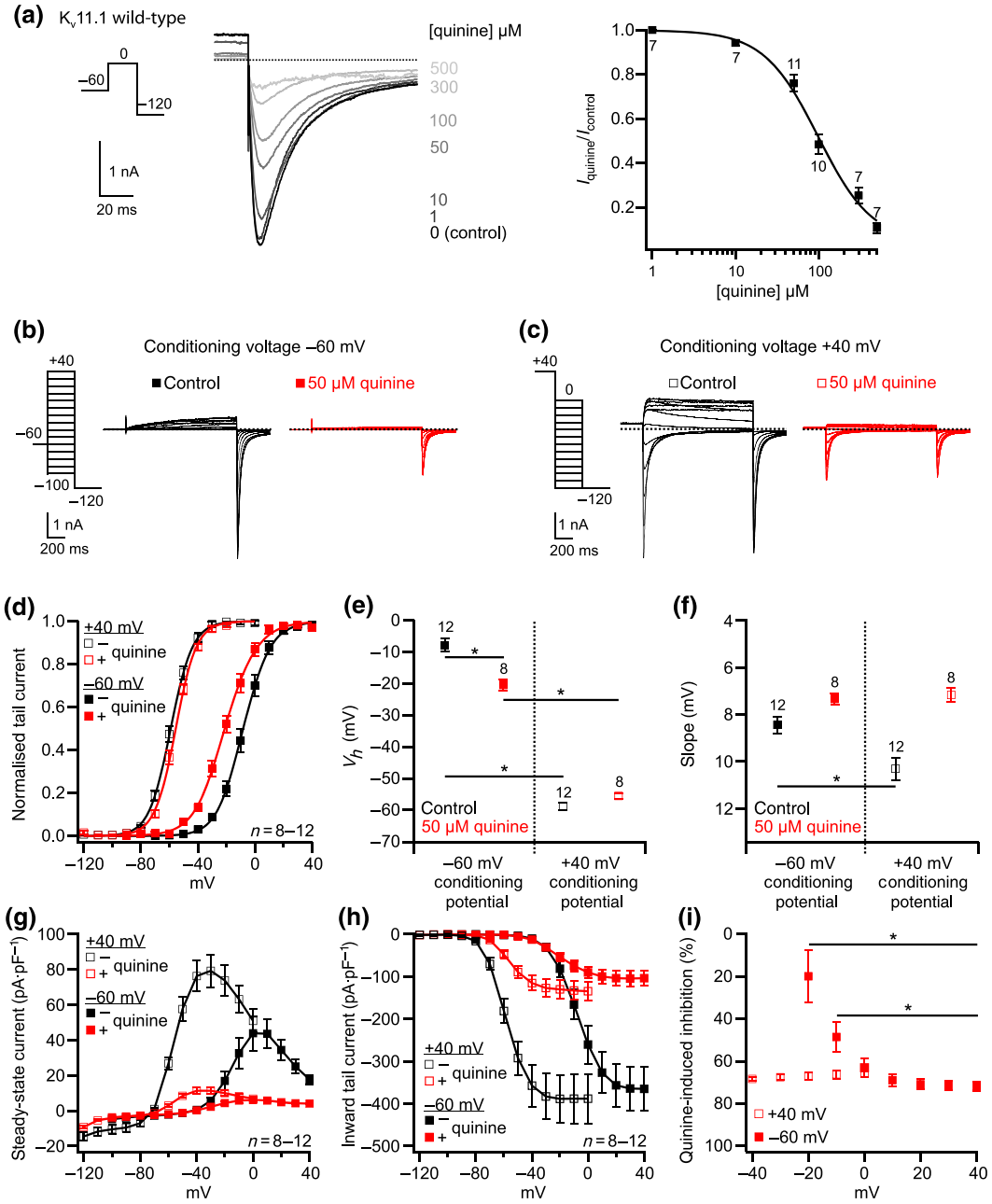

FIGURE 2 Voltage-dependent inhibition of $K_v11.1$ channels induced by quinine. (a) Quinine inhibited $K_v11.1$ channels transiently expressed in CHO cells in a concentration-dependent manner. The left panel shows representative recordings of a CHO cell expressing $K_v11.1$ treated with increasing quinine concentrations, the right panel depicts the summarised quinine dose–response relationship (IC_{50} and Hill coefficient calculated from a Hill fit to averaged data; solid line represents Hill fit). Scale bars, voltage protocol, quinine concentrations, and number of cells recorded as indicated. (b–f) After a conditioning potential of −60 mV, quinine induced activation of recombinant $K_v11.1$ channels at more negative membrane potentials. Representative recordings of $K_v11.1$ channels activated with voltage steps (as indicated) after conditioning voltage steps to (b) −60 mV or (c) +40 mV before (control) and at the end of the application of quinine (50 µM). (d) Summary of voltage-dependence of $K_v11.1$ channels derived from Boltzmann fits to individual recordings as shown in (b, c); solid line represents Boltzmann fit to averaged data. (e) Mean V_h of channel activation and (f) summarised slope factors of activation before and at the end of quinine application (50 µM; values derived from fits as shown in d). Quinine (1 mM) inhibited voltage-dependent (g) outward steady-state and (h) inward tail currents through recombinant $K_v11.1$ channels (current amplitudes analysed from recordings as shown in b, c). (i) Quinine-induced inhibition of $K_v11.1$ was voltage-dependent after conditioning potential of −60 mV but not after the depolarised conditioning potential of +40 mV (presented as % inhibition from data shown in g). *denotes significant differences

contrast to $K_v12.1$ wild-type channels, quinine block of $K_v12.1$(H462Y) was the same following both conditioning potentials and thus was independent on mode shift. Contrary to $K_v12.1$ wild-type, quinine (50 µM) shifted the voltage dependence of $K_v12.1$(H462Y) by −11 mV and −10 mV to hyperpolarised potentials after conditioning voltages of −60 mV and 0 mV respectively (Figure 4g–i).

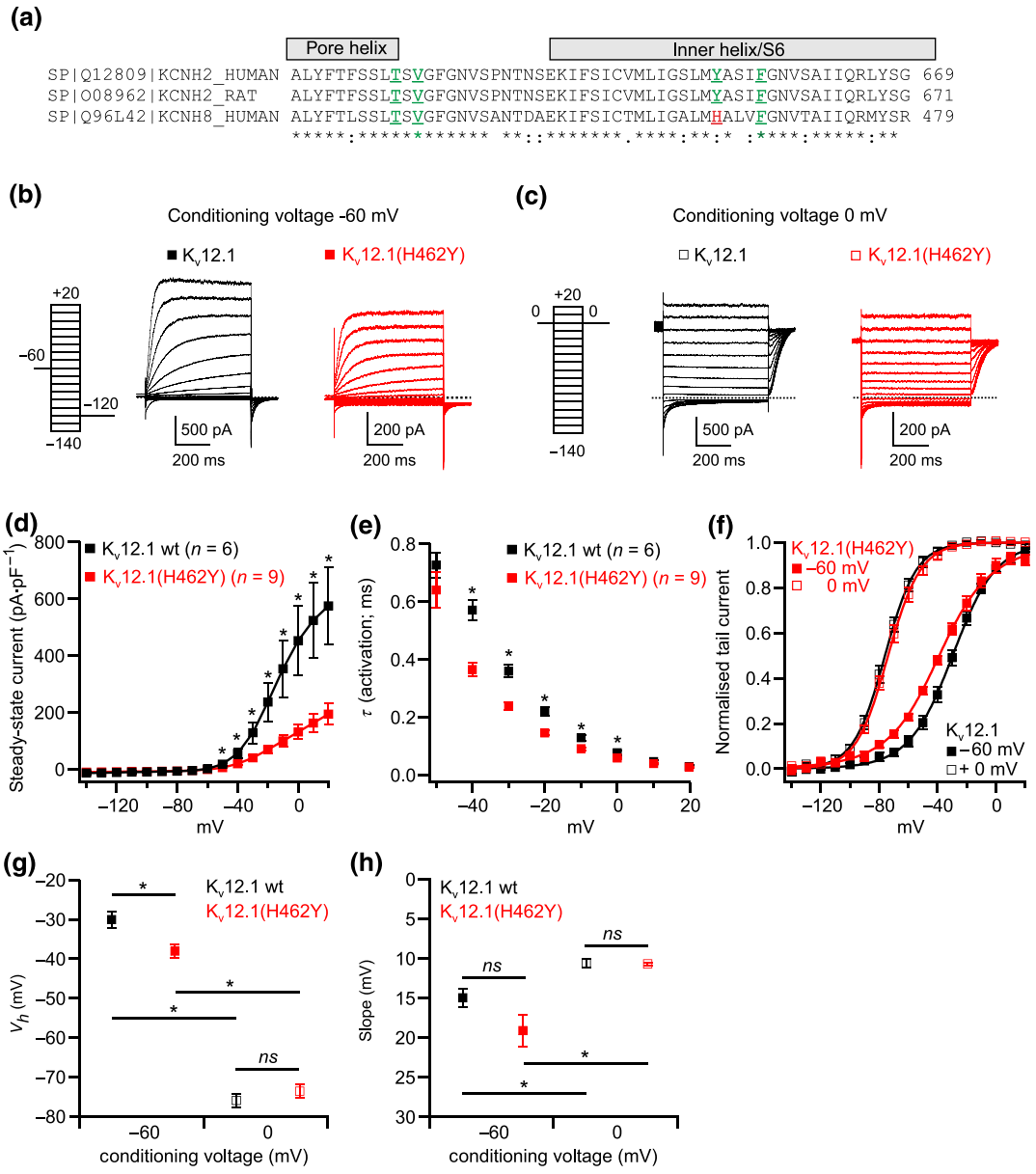

FIGURE 3 Characteristics of the $K_v12.1$(H462Y) channel mutant. (a) The panel shows an alignment of $K_v11.1$ isoforms from humans and rats (encoded by the *KCNH2* gene) with human $K_v12.1$ channels (*KCNH8* gene). Amino acids recently identified as important for quinoline-dependent inhibition of $K_v11.1$ channels are highlighted in colour (green, identical amino acids; red, amino acid exchange in $K_v12.1$; see text for details and references). Note that the quinine-binding "motif" of $K_v12.1$ differs only at one position from $K_v11.1$ channels. (b–h) Biophysical characteristics of $K_v12.1$(H462Y; red) in comparison with $K_v12.1$ wild-type channels (black). (b, c) Representative recordings of currents through $K_v12.1$ wild-type (black) and $K_v12.1$(H462Y; red) channels activated with the shown voltage protocols. (d) Steady-state outward currents through $K_v12.1$(H462Y) were significantly smaller than through $K_v12.1$ wild-type channels, and (e) $K_v12.1$(H462Y) activated significantly faster than wild-type channels, when activated through voltage steps between −40 and 0 mV (τ derived from monoexponential fits to activating current components in recordings shown in b, c). (f–h) $K_v12.1$(H462Y) activated at significantly more negative membrane potentials than wild-type channels after conditioning potential of −60 mV. (f) Summary of voltage-dependence of $K_v12.1$(H462Y) channels derived from Boltzmann fits to individual recordings as shown in (b, c); solid line represents Boltzmann fit to averaged data. (g) Mean V_h of channel activation and (h) summarised slope factors of activation (data on $K_v12.1$ wild-type channels are reproduced from Figure 1). *denotes significant differences

3.5 | $K_v12.1$(H462Y) channels exhibit $K_v11.1$-like quinine sensitivity

In summary, $K_v12.1$(H462Y) exhibited a 17 times higher quinine affinity than $K_v12.1$ wild-type, that is, quinine sensitivity of $K_v12.1$(H462Y) was more similar to $K_v11.1$ than to the wild-type channels (Figure 5a). Application of quinine induced opening of wild-type $K_v12.1$ channels at more positive potentials but at more negative values for $K_v12.1$(H462Y) and $K_v11.1$ (Figure 5b). Quinine inhibited $K_v12.1$ channels in a voltage-independent manner, but quinine block was

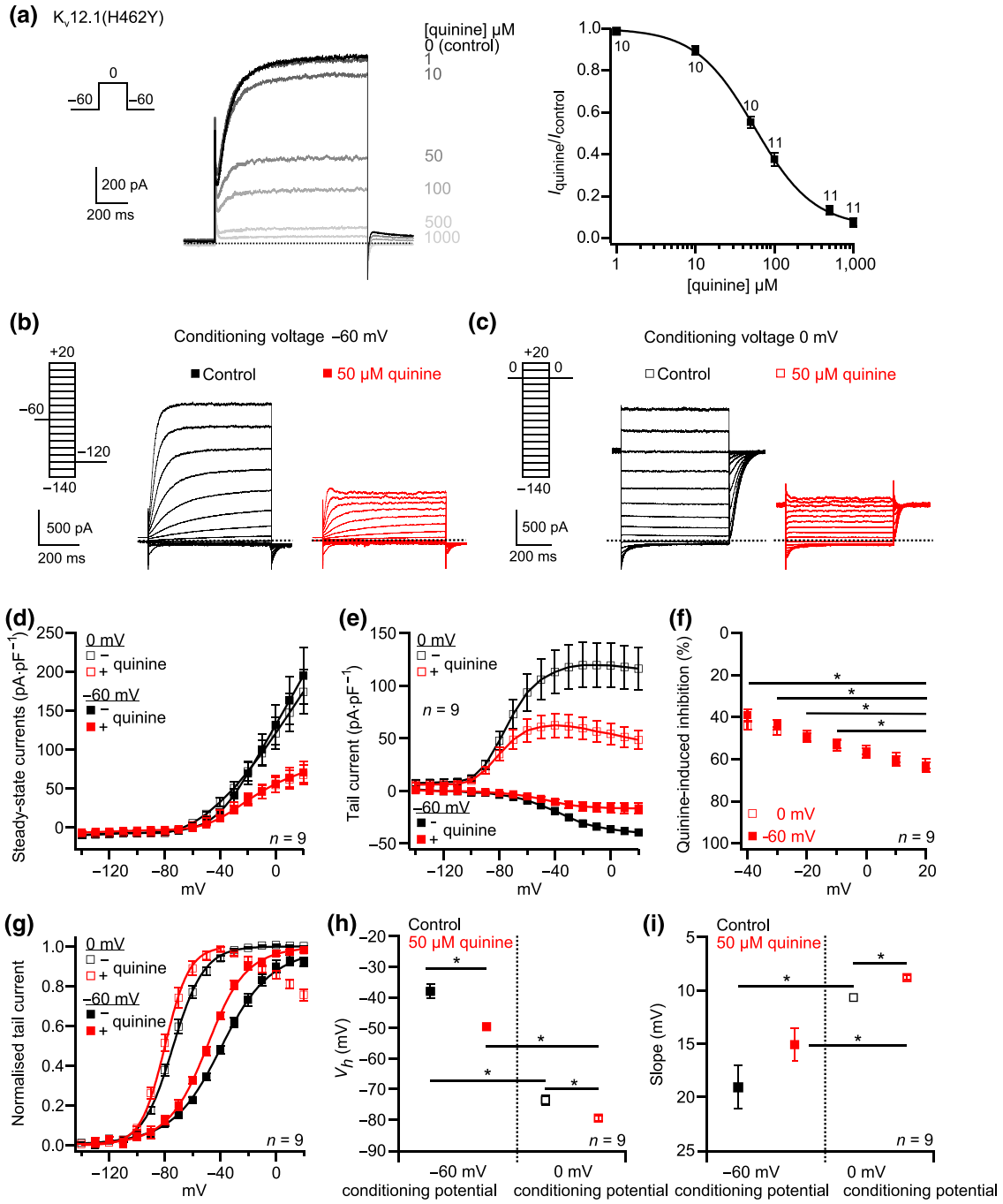

FIGURE 4 Voltage-dependent inhibition of K_v12.1(H462Y) channels through quinine at low concentrations. (a) Extracellular application of quinine inhibited K_v12.1(H462Y) channels overexpressed in CHO cells. The panel shows representative recordings of a CHO cell expressing K_v12.1(H462Y) treated with increasing quinine concentrations (left) and the summarised dose–response relationship (right; IC_{50} and Hill coefficient were calculated from a Hill fit to averaged recordings as shown in the left panel; solid line represents Hill fit). Scale bars, voltage protocol, quinine concentrations, and number or cells recorded as indicated. (b–i) Quinine inhibited inward and outward currents through K_v12.1(H462Y) channels and induced channel activation at more negative membrane potentials. Representative recordings of recombinant K_v12.1 channels activated by voltage steps between −140 and +20 mV following 200-ms conditioning voltage steps to (b) −60 mV or (c) 0 mV before (black) and at the end of quinine application (50 µM; red). Summarised voltage-dependent (d) steady-state currents and (e) inward tail currents through K_v12.1(H462Y) before (black) and at the end of quinine treatment (50 µM; current amplitudes analysed from recordings as shown in b, c). (f) Quinine-induced inhibition of K_v12.1(H462Y) was voltage-dependent (presented as % inhibition from data shown in d). (g–i) Summary of voltage-dependence of K_v12.1(H462Y) channels derived from Boltzmann fits to individual recordings as shown in (b, c); solid line represents Boltzmann fit to averaged data. (h) Mean V_h of channel activation and (i) summarised slope factors of activation before and at the end of treatment with quinine (50 µM; values derived from fits as shown in g). *denotes significant differences

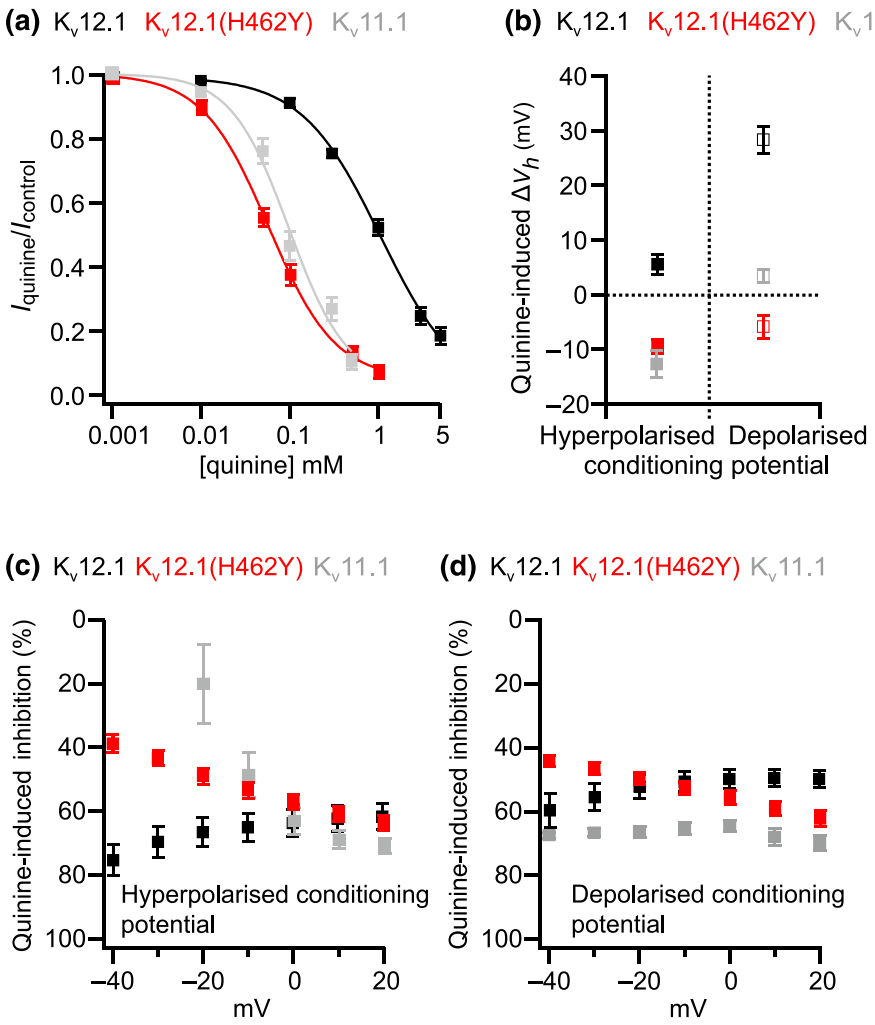

FIGURE 5 The inhibition induced by quinine of K_v12.1(H462Y) channels shows K_v11.1-like characteristics. This figure summarises our findings on K_v12.1 wild-type channels and H462Y mutant as well as on K_v11.1 wild-type channels (data are reproduced from Figures 1–4). (a) The affinity of K_v12.1(H462Y) for quinine was 17-fold higher than that of the wild-type and accordingly very similar to K_v11.1. (b) Quinine induced activation of K_v12.1 channels at more positive potentials following the hyperpolarised (−60 mV) and the depolarised conditioning potential (0 mV). In contrast, K_v12.1(H462Y) and K_v11.1 channels activated at more negative membrane potentials in the presence of quinine following the hyperpolarised conditioning potential. Only slight changes of voltage-dependence of K_v12.1(H462Y) and K_v11.1 channels were detected during application of quinine following the depolarised conditioning potential. (c, d) Quinine-mediated block was voltage-independent for K_v12.1 but voltage-dependent for K_v12.1(H462Y). Note that quinine inhibition of K_v11.1 channels was voltage-dependent only following the hyperpolarised conditioning potential. Summaries of quinine-induced inhibition (% of controls) for (c) the hyperpolarised and for (d) the depolarised conditioning membrane potential. Quinine was applied at 1 mM for K_v12.1 channels and at 50 μM for K_v12.1(H462Y) and K_v11.1. Mode shift was induced through conditioning potentials of −60 and 0 mV for K_v12.1 isoforms and at −60 and +40 mV for K_v11.1 channels

completely voltage dependent for K_v12.1(H462Y) and partially voltage dependent (after hyperpolarised conditioning potentials) for K_v11.1 channels (Figure 5c,d). In contrast to K_v12.1(H462Y), K_v12.1 wild-type channels apparently were more sensitive to quinine after conditioning hyperpolarisation of the membrane (c.f. Figure 1i), that is, for K_v12.1 wild-type channels, quinine-induced inhibition depended on mode shift (just as for K_v11.1 channels). Accordingly, closely related K_v12.1 and K_v11.1 channels exhibited markedly different quinine sensitivity and characteristics of inhibition, but introduction of the H462Y amino acid exchange conferred K_v11.1-like quinine sensitivity to K_v12.1 channels. Based on these findings, we conclude that H462 determines the low quinine sensitivity and the characteristics of quinine-dependent inhibition for K_v12.1 channels and that the binding pocket for substituted quinolines in the central cavity is not completely conserved within the Eag superfamily of K_v channels. However, as the H462Y point mutation restored K_v11.1-like quinine sensitivity in K_v12.1, these findings demonstrated that the quinoline-binding pocket also exists in K_v12.1 and that thus the overall architecture of the channels is similar.

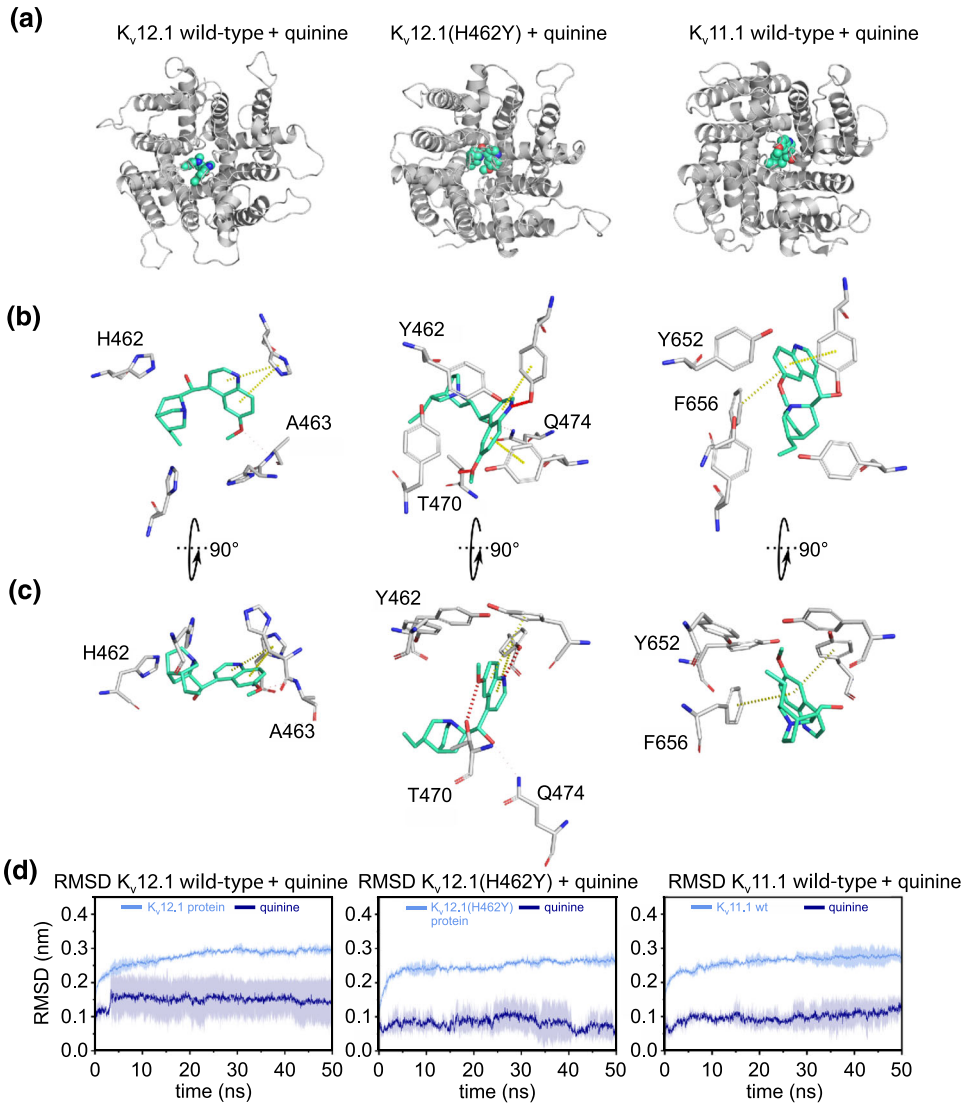

FIGURE 6 Molecular interactions of quinine with $K_v12.1$, $K_v12.1$(H462Y), and $K_v11.1$. (a) Top-view representations of $K_v12.1$ (left), $K_v12.1$(H462Y; middle), and $K_v11.1$ (right) channels with docked quinine (green–cyan spheres). (b) Top and (c) side view of the quinine-binding site after 50 ns of molecular dynamics simulations for $K_v12.1$ (left), $K_v12.1$(H462Y; middle), and $K_v11.1$ (right). Directly interacting residues, as well as position 462 in $K_v12.1$ isoforms (652 in $K_v11.1$), are presented as sticks, with oxygen atoms coloured in red and nitrogen atoms coloured in blue. Yellow lines indicate π-stacking interactions, while red lines indicate H bonds. (d) Stability of the pore domains (excluding extracellular loops), measured as the root-mean-square deviation (RMSD) as a function of 50-ns simulation time

3.6 | H462 determines the low quinine affinity of human $K_v12.1$ channels

To elucidate the molecular principles of the low quinine affinity of $K_v12.1$, we performed molecular docking and subsequent MD analyses (Figure 6). Quinine binding to the pore helix/S6 domain (amino acids S353–Y477) of $K_v12.1$ and $K_v12.1$(H462Y) channels was studied using homology models based on the cryo-EM structure of human $K_v11.1$ (Wang & MacKinnon, 2017). We also utilised the available structural information to study quinine binding to $K_v11.1$ channels. Molecular docking suggested that quinine binds below residue H462 into the central cavity of human $K_v12.1$ (Figure 6a, left panel), with an estimated binding affinity (Chemscore.DG) of −20.5 kJ·mol^{-1}. To validate the stability and refine the binding pose obtained from docking, we performed three independent 50-ns MD simulations of the highest scored docking pose. Overall, quinine remained stable in these MD simulations, as indicated by root-mean-square deviation (RMSD) below 2 Å (Figure 6d, left panel). Further, π–π stacking between methoxyquinoline group and H462 from one subunit was maintained throughout 50 ns of MD simulation (Figure 6 b,c, left panel). Similar to wild-type channels, quinine docked into the central cavity of $K_v12.1$(H462Y) without any obvious interactions to the residues of the selectivity filter (Figure 6a–c, middle panel). In $K_v12.1$(H462Y), π–π interactions with the methoxyquinoline moiety were also observed; however, in the mutant channel, these interactions are formed with mutated Y462 side chains from two adjacent subunits. Additionally, we observed a hydrogen bond between Y462 and quinoline moiety of quinine in the majority of docking poses that

remained stable throughout the 50-ns MD simulations. In agreement with our experimental findings, the estimated quinine-binding affinity of −31.1 kJ·mol^{-1} for K_v12.1(H462Y) was considerably higher than for wild-type K_v12.1 channels. In line, in the simulations, an additional hydrogen bond between the methoxy group of quinidine and the residue T470 formed in the mutant channels (Figure 6c, middle panel). As shown in Figure 6d, the binding pose of quinine was highly stable in MD simulations, with an RMSD of about 1 Å. In the K_v11.1 cryo-EM structure (Wang & MacKinnon, 2017), quinine was also predicted to bind slightly below Y652, in the central cavity, with favourable hydrophobic interactions with Y652 residues of all subunits and with F656 from only one subunit. Also, in line with our experimental findings, the estimated affinity of quinine binding to K_v11.1 wild-type channels amounts to −33.9 kJ·mol^{-1} in our simulations and thus was similar to K_v12.1(H462Y) and higher than that of wild-type K_v12.1 channels. Further, π−π interactions with Y652 and F656 residues in K_v11.1 from opposite subunits were predicted by these simulations (Figure 6b,c, right panel), again leading to a very stable binding mode with RMSD values of ~1 Å (Figure 6d, right panel).

In summary, molecular modelling revealed that weak interactions between quinine and particularly H462 determined the low affinity and sensitivity of K_v12.1 wild-type channels to quinine. The higher affinity of K_v12.1(H462Y) channels and of the closely related K_v11.1 can be explained by more favourable interactions with the drug, mainly at position Y462, and in the case of K_v11.1 additionally with F656 from one subunit. Surprisingly, despite the conservation of this second aromatic side chain between K_v11 and K_v12 channels, interactions with this second aromatic residue are completely absent in the K_v12.1 (Figure 6b, left panel vs. right panel). However, also in K_v11.1 channels, these interactions are relatively weak due to a preferred orientation of the Y652/F656 side chains towards helix S5 (see Figure S2, for orientation of aromatic side chains at positions H462/F466 in K_v12.1 wild-type and Y652/F656 in K_v11.1 wild-type channels in simulations).

4 | DISCUSSION

Substituted quinolines are well-known antimalarial agents (quinine and chloroquine) and antiarrhythmic drugs (quinidine; Bozic, Uzelac, Kezic, & Bajcetic, 2018). As considerable side effect, these substances inhibit K_v11.1 channels at low micromolar concentrations, which may result in acquired (drug-induced) LQT syndrome, syncope, and sudden death in humans (Mitcheson et al., 2005; Mitcheson et al., 2000; Sanguinetti & Tristani-Firouzi, 2006). Several mutagenesis studies have attributed the susceptibility of K_v11.1 to drug-dependent block to amino acids in the pore domain of these channels, threonine 623 and valine 625 of inner pore helix and selectivity filter, respectively, as well as tyrosine 652 and phenylalanine 656 in the sixth transmembrane segment (S6; Mitcheson et al., 2000; Sanchez-Chapula et al., 2002; Sanchez-Chapula et al., 2003). On the one hand, valine 625 (together with other residues such as asparagine 588, serine 631, and serine 620) controls drug sensitivity of K_v11.1 through its contribution to channel inactivation that has been shown to be necessary for channel inhibition by several high-affinity blockers (e.g., Kamiya et al., 2006; Perrin et al., 2008; Wu et al., 2015). On the other hand, some of these residues form hydrophobic pockets in combination with other amino acids at the inner surface of the small central cavity of K_v11.1 channels (Wang & MacKinnon, 2017). These pockets are endowed with high electronegative potentials and therefore favour binding of positively charged drugs (Wang & MacKinnon, 2017). The exclusive sensitivity of K_v11.1 to a wide variety of drugs with diverging structures is explained by the absence of such binding pockets in other K^+ channels (Wang & MacKinnon, 2017).

Closely related K_v10 and K_v12 channels share high similarity to K_v11.1, which suggests that these channels also possess analogous drug-binding pockets, similar drug sensitivity, and characteristics of inhibition (Bauer & Schwarz, 2018). Indeed, the respective amino acids determining the susceptibility of K_v11.1 to quinoline block are conserved in K_v10 channels. However, whereas K_v10.1 displayed the same sensitivity to quinidine-dependent inhibition as K_v11.1, quinidine sensitivity of K_v10.2 channels was 100-fold lower (Gessner et al., 2004; Lees-Miller et al., 2000; Sanchez-Chapula et al., 2003; Schonherr et al., 2002). The lower susceptibility of the K_v10 isoforms to drug-induced inhibition is explained by their lack of inactivation, that is, conformational reorientations during inactivation necessary for high affinity drug block in K_v11.1 do not occur in K_v10 channels (Chen et al., 2002; Ficker et al., 1998; Ficker et al., 2001). Thus, the lower sensitivity of K_v10 channels indicates that additional drug interaction sites outside the central binding motif might determine drug block in these channels (Gessner et al., 2004; Schonherr et al., 2002). We wondered whether K_v12.1 channels possess a quinoline-binding pocket analogous to K_v10.1 and K_v11.1 channels despite an amino acid exchange at position 462. We found that quinine inhibited K_v12.1 channels, but their sensitivity was 10 times lower than that of K_v11.1 channels. Thus, K_v12.1 constitutes a natural variant of Eag superfamily channels with low quinoline-binding affinity.

4.1 | H462 determines quinine sensitivity of K_v12.1

The quinoline-binding "motif" of K_v11.1 is not completely conserved in the three members of the K_v12 channel family that carry a histidine at the position homologous to tyrosine 652 in K_v11.1 (H462 in K_v12.1; c.f. Figure 3a). As in K_v11.1, this aromatic residue determines the quinoline-binding affinity (Lees-Miller et al., 2000; Sanchez-Chapula et al., 2003), we hypothesised that this small sequence difference explained the 10-fold lower quinine sensitivity of K_v12.1. Indeed, replacing this histidine in K_v12.1 with the respective tyrosine of K_v11.1 through site-directed mutagenesis dramatically increased the quinine affinity of K_v12.1(H462Y). In fact, quinine sensitivity of K_v12.1(H462Y) was more similar to K_v11.1 than to wild-type K_v12.1. Our findings are supported by earlier studies showing that mutating Y652 dramatically changes quinidine sensitivity of K_v11.1 channels,

for example, introduction of an alanine at this position caused a threefold reduction of quinidine affinity in K_v11.1(Y652A) channels (Sanchez-Chapula et al., 2003). Utilising molecular modelling simulations, we found that the low sensitivity of K_v12.1 channels may be explained by only weak interactions between quinine and amino acids in the central cavity (including H462). Noteworthy, in K_v12.1(H462Y) channels, more favourable interactions developed that most probably rendered this channel mutant more sensitive to quinine. In line with our experimental findings, docking analyses predicted considerably lower quinine affinities for K_v12.1 (−20.5 kJ·mol^{-1}), compared with the K_v12.1(H462Y) mutant (−31.1 kJ·mol^{-1}) and K_v11.1 wild-type channels (−33.9 kJ·mol^{-1}). Our models predicted a key difference in the orientation and interactions of the first aromatic side chain, which limits hydrophobic and π–π interactions in K_v12, while providing strong interactions in K_v11 channels. Taking together, our findings are in good agreement with a hypothesis previously published by the Sanguinetti group (Chen et al., 2002). Thus, our modelling approach recapitulated experimental findings on K_v11.1 (Sanchez-Chapula et al., 2003) and provided a ready and straightforward explanation for the higher quinine affinity of K_v11.1 and K_v12.1(H462Y) compared with K_v12.1 wild-type channels.

Yet, as mentioned above, drug sensitivity of K_v11.1 channels is determined by channel inactivation (e.g., through V625, N588, S631, and S620; Ficker et al., 1998; Ficker et al., 2001; Kamiya et al., 2006; Perrin et al., 2008; Wu et al., 2015). As shown for K_v10 channels (Chen et al., 2002; Ficker et al., 1998; Ficker et al., 2001), lack of inactivation might contribute to low drug sensitivity of K_v12.1 channels. However, above-mentioned residues (except N588 where K_v12.1 has an E) are conserved in K_v12.1 channels, and the single amino acid exchange H462Y sufficed to significantly lower the quinine affinity of these channels (even slightly below that of K_v11.1 channels; c.f. Figure 5a). We thus estimate that relevance of these amino acids for drug interactions is low in K_v12.1, but we cannot provide any evidence for this assumption at present. Thus, further work is needed to elucidate whether these residues also determine drug sensitivity in K_v12 family members and whether the channel mutant inactivates at all (e.g., during prolonged depolarisations).

Importantly, our findings once again highlight that Y652 determines quinoline sensitivity in closely related K_v11.1 channels (Lees-Miller et al., 2000; Macdonald, Kim, Kurata, & Fedida, 2018; Sanchez-Chapula et al., 2002; Sanchez-Chapula et al., 2003). Although indicated by an early report analysing binding of chloroquine to K_v11.1 in silico (Sanchez-Chapula et al., 2002), we did not detect any cation–π interactions between quinine and K_v11.1, K_v12.1, or K_v12.1(H462Y) channels. Noteworthy, our simulations support a recent study that utilised unnatural amino acid incorporation to show that cation–π interactions at position Y652 are not relevant for drug binding in K_v11.1 channels (Macdonald et al., 2018). Based on these findings, we conclude that H462 determines the low quinine sensitivity of K_v12.1 and that possibly no amino acid motifs outside the central cavity contribute to quinoline binding in K_v12.1 channels (for K_v10, see Gessner et al., 2004; Schonherr et al., 2002). Thus, as far as quinoline sensitivity is concerned, K_v12 channels are probably more similar to other K_v families that typically carry isoleucine or valine at this position than to closely related K_v11 channels.

4.2 | H462 determines characteristics of quinine-dependent inhibition in K_v12.1

Our experiments showed that quinine-induced inhibition of K_v12.1 channels was largely voltage independent and characterised by a shift of activation voltages to depolarised potentials. Although it has been shown that many inhibitors (including quinidine or chloroquine; Sanchez-Chapula et al., 2003; Sanchez-Chapula et al., 2002) preferentially block activated K_v11.1 channels, we did not find any evidence for such quinine-dependent open channel block for K_v12.1 wild-type channels. Transient activation of K_v12.1(H462Y) channels at depolarised membrane potentials in the presence of quinine (c.f. Figure 4b), however, might indicate such open channel block for the channel mutant, but we consider that further work including other inhibitors is needed to elucidate whether the amino acid position 462 indeed determines open channel block in K_v12.1 channels.

As K_v12.1 wild-type channels were more sensitive to quinine after conditioning hyperpolarisation of the membrane, quinine block depended on mode shift, in contrast to K_v12.1(H462Y) that were inhibited by quinine independent on conditioning potentials. Although we do not have any evidence for this assumption yet, conformational changes associated with establishment of mode shift might thus render K_v12.1 channels less sensitive to quinine. Quinine inhibited K_v11.1 more significantly, when the channels were activated at depolarised potentials, but only following the hyperpolarised conditioning potential. Thus, quinine block of K_v11.1 also depended on mode shift, but the underlying mechanisms may be different between K_v11 and K_v12 channels. In contrast to K_v12.1 wild-type channels, quinine induced K_v11.1 channel opening at more negative membrane potentials in line with a previous report (Sanchez-Chapula et al., 2003). Interestingly, the H462Y amino acid exchange conferred K_v11.1-type characteristics of quinine-dependent inhibition to K_v12.1 channels. Thus, H462 determines not only quinine sensitivity but also the characteristics of quinine-dependent inhibition in K_v12.1 channels. Likewise, mutating the homologous tyrosine substantially changed the voltage dependence of quinoline block in K_v11.1, that is, voltage dependence was abolished in K_v11.1(Y652F), but it was completely reversed in K_v11.1(Y652A) channels (Sanchez-Chapula et al., 2003). Yet the molecular mechanisms underlying such voltage-dependent inhibition remain elusive for the K_v12.1 mutant, as well as for K_v11.1 channels. It was hypothesised earlier for chloroquine-induced block of K_v11.1 that Y652 might change position during voltage-dependent gating, thereby generating a depolarisation-induced binding pocket with higher affinity (Sanchez-Chapula et al., 2003). This may induce pronounced channel inhibition during channel activation at more depolarised membrane potentials. Accordingly, as proposed for K_v11.1 carrying mutations at position 652 (Sanchez-Chapula et al., 2003), the low quinine affinity of K_v12.1 wild-type

channels might prevent generation of an analogous binding site with higher affinity, which might account for lack of voltage dependence in these channels. Thus, similar molecular mechanisms may apply for K_v11.1 and K_v12.1 during drug-induced inhibition, but we cannot provide any evidence for such processes at present.

4.3 | Conclusion and significance

We showed that K_v12.1 is a natural variant of Eag superfamily channels with low quinine sensitivity. Thus, the drug-binding pocket in the central cavity is not completely conserved in the Eag superfamily of K_v channels, which highlights functional and pharmacological diversity within this group of evolutionary conserved ion channels. However, our work also demonstrated that the drug-binding pocket exists in K_v12.1 and that thus the overall architecture of the channels is similar. Further work is needed to elucidate whether K_v12.1 channels are also endowed with lower sensitivity to the many more drugs that block closely related K_v11.1.

ACKNOWLEDGEMENTS

The authors gratefully acknowledge the kind gift of plasmids for K_v12.1 from Dr T. Jegla and for K_v11.1 from Dr. C.K. Bauer. We thank Olga Ebers for superb technical assistance.

This work was funded by the Deutsche Forschungsgemeinschaft (DFG Priority Program 1608: "Ultrafast and temporally precise information processing: Normal and dysfunctional hearing," [LE 3600/1-1 to M.G.L.]).

W.B.V.H. was supported by an internship from the Graduate School of Life Sciences from the University of Utrecht and a travel grant from the Dutch Heart Foundation.

The computational results presented have been achieved in part using the Vienna Scientific Cluster (VSC).

CONFLICT OF INTEREST

The authors declare no conflict of interest.

AUTHOR CONTRIBUTIONS

M.D., A.S.-W., and M.G.L. participated in the research design; M.D., W.B.V.H., A.S.-W., and M.G.L. conducted the experiments and performed the data analysis; M.D., A.S.-W., and M.G.L. wrote or contributed to the writing of the manuscript; and all authors approved the final version of the manuscript.

DECLARATION OF TRANSPARENCY AND SCIENTIFIC RIGOUR

This Declaration acknowledges that this paper adheres to the principles for transparent reporting and scientific rigour of preclinical research as stated in the *BJP* guidelines for Design & Analysis and as recommended by funding agencies, publishers, and other organisations engaged with supporting research.

ORCID

Michael G. Leitner https://orcid.org/0000-0002-3259-6481

REFERENCES

Abraham, M. J., van der Spoel, D., Lindahl, E., Hess, B., & team atGd (2016). GROMACS user manual version 5.1.2, www.gromacs.org.

Alexander, S. P., Striessnig, J., Kelly, E., Marrion, N. V., Peters, J. A., Faccenda, E., … CGTP Collaborators. (2017). The Concise Guide to PHARMACOLOGY 2017/18: Voltage-gated ion channels. *British Journal of Pharmacology*, *174*(Suppl 1), S160–S194. https://doi.org/10.1111/bph.13884

Bauer, C. K., & Schwarz, J. R. (2001). Physiology of EAG K^+ channels. *The Journal of Membrane Biology*, *182*, 1–15. https://doi.org/10.1007/s00232-001-0031-3

Bauer, C. K., & Schwarz, J. R. (2018). Ether-a-go-go K^+ channels: Effective modulators of neuronal excitability. *The Journal of Physiology*, *596*, 769–783. https://doi.org/10.1113/JP275477

Best, R. B., Zhu, X., Shim, J., Lopes, P. E., Mittal, J., Feig, M., & MacKerell, A. D. Jr. (2012). Optimization of the additive CHARMM all-atom protein force field targeting improved sampling of the backbone φ, ψ and side-chain χ_1 and χ_2 dihedral angles. *Journal of Chemical Theory and Computation*, *8*, 3257–3273. https://doi.org/10.1021/ct300400x

Bezanilla, F., Taylor, R. E., & Fernandez, J. M. (1982). Distribution and kinetics of membrane dielectric polarization. 1. Long-term inactivation of gating currents. *The Journal of General Physiology*, *79*, 21–40. https://doi.org/10.1085/jgp.79.1.21

Bozic, B., Uzelac, T. V., Kezic, A., & Bajcetic, M. (2018). The role of quinidine in the pharmacological therapy of ventricular arrhythmias 'quinidine'. *Mini Reviews in Medicinal Chemistry*, *18*, 468–475. https://doi.org/10.2174/1389557517666170707110450

Bussi, G., Donadio, D., & Parrinello, M. (2007). Canonical sampling through velocity rescaling. *The Journal of Chemical Physics*, *126*, 014101. https://doi.org/10.1063/1.2408420

Chen, J., Seebohm, G., & Sanguinetti, M. C. (2002). Position of aromatic residues in the S6 domain, not inactivation, dictates cisapride sensitivity of HERG and eag potassium channels. *Proceedings of the National Academy of Sciences of the United States of America*, *99*, 12461–12466. https://doi.org/10.1073/pnas.192367299

Curran, M. E., Splawski, I., Timothy, K. W., Vincent, G. M., Green, E. D., & Keating, M. T. (1995). A molecular basis for cardiac arrhythmia: HERG mutations cause long QT syndrome. *Cell*, *80*, 795–803. https://doi.org/10.1016/0092-8674(95)90358-5

Curtis, M. J., Alexander, S., Cirino, G., Docherty, J. R., George, C. H., Giembycz, M. A., … Ahluwalia, A. (2018). Experimental design and analysis and their reporting II: updated and simplified guidance for authors and peer reviewers. *British Journal of Pharmacology*, *175*, 987–993. https/doi.org/10.1111/bph.14153

Dai, G., & Zagotta, W. N. (2017). Molecular mechanism of voltage-dependent potentiation of KCNH potassium channels. *eLife*, *6*. https://doi.org/10.7554/eLife.26355

Darden, T., York, D., & Pedersen, L. (1993). Particle mesh Ewald: An *N*·log(*N*) method for Ewald sums in large systems. *The Journal of Chemical Physics*, *98*, 10089–10092. https://doi.org/10.1063/1.464397

Dierich, M., Evers, S., Wilke, B. U., & Leitner, M. G. (2018). Inverse modulation of neuronal K_v12.1 and K_v11.1 channels by 4-aminopyridine and NS1643. *Frontiers in Molecular Neuroscience*, *11*, 11. https://doi.org/10.3389/fnmol.2018.00011

Dierich, M., & Leitner, M. G. (2018). K_v12.1 channels are not sensitive to G_qPCR-triggered activation of phospholipase Cβ. *Channels (Austin, Tex.)*, *12*, 228–239. https://doi.org/10.1080/19336950.2018.1475783

Engeland, B., Neu, A., Ludwig, J., Roeper, J., & Pongs, O. (1998). Cloning and functional expression of rat ether-a-go-go-like K^+ channel genes. *The Journal of Physiology*, *513* (Pt 3, 647–654. https://doi.org/10.1111/j.1469-7793.1998.647ba.x

Ficker, E., Jarolimek, W., & Brown, A. M. (2001). Molecular determinants of inactivation and dofetilide block in ether a-go-go (EAG) channels and EAG-related K^+ channels. *Molecular Pharmacology*, *60*, 1343–1348. https://doi.org/10.1124/mol.60.6.1343

Ficker, E., Jarolimek, W., Kiehn, J., Baumann, A., & Brown, A. M. (1998). Molecular determinants of dofetilide block of HERG K^+ channels. *Circulation Research*, *82*, 386–395. https://doi.org/10.1161/01.RES.82.3.386

Furutani, K., Yamakawa, Y., Inanobe, A., Iwata, M., Ohno, Y., & Kurachi, Y. (2011). A mechanism underlying compound-induced voltage shift in the current activation of hERG by antiarrhythmic agents. *Biochemical and Biophysical Research Communications*, *415*, 141–146. https://doi.org/10.1016/j.bbrc.2011.10.034

Gessner, G., Zacharias, M., Bechstedt, S., Schonherr, R., & Heinemann, S. H. (2004). Molecular determinants for high-affinity block of human EAG potassium channels by antiarrhythmic agents. *Molecular Pharmacology*, *65*, 1120–1129. https://doi.org/10.1124/mol.65.5.1120

Harding, S. D., Sharman, J. L., Faccenda, E., Southan, C., Pawson, A. J., Ireland, S., … NC-IUPHAR (2018). The IUPHAR/BPS Guide to PHARMACOLOGY in 2018: Updates and expansion to encompass the new guide to IMMUNOPHARMACOLOGY. *Nucleic Acids Research*, *46*, D1091–D1106. https://doi.org/10.1093/nar/gkx1121

Helliwell, M. V., Zhang, Y., El Harchi, A., Du, C., Hancox, J. C., & Dempsey, C. E. (2018). Structural implications of hERG K^+ channel block by a high-affinity minimally structured blocker. *Journal of Biological Chemistry*, *293*, 7040–7057. https://doi.org/10.1074/jbc.RA117.000363

Hess, B., Bekker, H., Berendsen, H. J. C., & Fraaije, J. (1997). LINCS: A linear constraint solver for molecular simulations. *Journal of Computational Chemistry*, *18*, 1463–1472. https://doi.org/10.1002/(SICI)1096-987X(199709)18:12<1463::AID-JCC4>3.0.CO;2-H

Humphrey, W., Dalke, A., & Schulten, K. (1996). VMD: Visual molecular dynamics. *Journal of Molecular Graphics & Modelling*, *14*, 33–38. https://doi.org/10.1016/0263-7855(96)00018-5

Jo, S., Kim, T., Iyer, V. G., & Im, W. (2008). CHARMM-GUI: A web-based graphical user interface for CHARMM. *Journal of Computational Chemistry*, *29*, 1859–1865. https://doi.org/10.1002/jcc.20945

Jones, G., Willett, P., Glen, R. C., Leach, A. R., & Taylor, R. (1997). Development and validation of a genetic algorithm for flexible docking. *Journal of Molecular Biology*, *267*, 727–748. https://doi.org/10.1006/jmbi.1996.0897

Kamiya, K., Mitcheson, J. S., Yasui, K., Kodama, I., & Sanguinetti, M. C. (2001). Open channel block of HERG K^+ channels by vesnarinone. *Molecular Pharmacology*, *60*, 244–253. https://doi.org/10.1124/mol.60.2.244

Kamiya, K., Niwa, R., Mitcheson, J. S., & Sanguinetti, M. C. (2006). Molecular determinants of HERG channel block. *Molecular Pharmacology*, *69*, 1709–1716. https://doi.org/10.1124/mol.105.020990

Kazmierczak, M., Zhang, X., Chen, B., Mulkey, D. K., Shi, Y., Wagner, P. G., … Jegla, T. (2013). External pH modulates EAG superfamily K^+ channels through EAG-specific acidic residues in the voltage sensor. *The Journal of General Physiology*, *141*, 721–735. https://doi.org/10.1085/jgp.201210938

Keating, M. T., & Sanguinetti, M. C. (2001). Molecular and cellular mechanisms of cardiac arrhythmias. *Cell*, *104*, 569–580. https://doi.org/10.1016/S0092-8674(01)00243-4

Klauda, J. B., Venable, R. M., Freites, J. A., O'Connor, J. W., Tobias, D. J., Mondragon-Ramirez, C., … Pastor, R. W. (2010). Update of the CHARMM all-atom additive force field for lipids: Validation on six lipid types. *The Journal of Physical Chemistry. B*, *114*, 7830–7843. https://doi.org/10.1021/jp101759q

Lees-Miller, J. P., Duan, Y., Teng, G. Q., & Duff, H. J. (2000). Molecular determinant of high-affinity dofetilide binding to HERG1 expressed in *Xenopus* oocytes: Involvement of S6 sites. *Molecular Pharmacology*, *57*, 367–374.

Leitner, M. G., Feuer, A., Ebers, O., Schreiber, D. N., Halaszovich, C. R., & Oliver, D. (2012). Restoration of ion channel function in deafness-causing KCNQ4 mutants by synthetic channel openers. *British Journal of Pharmacology*, *165*, 2244–2259. https://doi.org/10.1111/j.1476-5381.2011.01697.x

Leitner, M. G., Halaszovich, C. R., & Oliver, D. (2011). Aminoglycosides inhibit KCNQ4 channels in cochlear outer hair cells via depletion of phosphatidylinositol(4,5)bisphosphate. *Molecular Pharmacology*, *79*, 51–60. https://doi.org/10.1124/mol.110.068130

Leitner, M. G., Michel, N., Behrendt, M., Dierich, M., Dembla, S., Wilke, B. U., … Oliver, D. (2016). Direct modulation of TRPM4 and TRPM3 channels by the phospholipase C inhibitor U73122. *British Journal of Pharmacology*, *173*, 2555–2569. https://doi.org/10.1111/bph.13538

Li, X., Anishkin, A., Liu, H., van Rossum, D. B., Chintapalli, S. V., Sassic, J. K., … Jegla, T. (2015). Bimodal regulation of an Elk subfamily K^+ channel by phosphatidylinositol 4,5-bisphosphate. *The Journal of General Physiology*, *146*, 357–374. https://doi.org/10.1085/jgp.201511491

Macdonald, L. C., Kim, R. Y., Kurata, H. T., & Fedida, D. (2018). Probing the molecular basis of hERG drug block with unnatural amino acids. *Scientific Reports*, *8*, 289. https://doi.org/10.1038/s41598-017-18448-x

MacKerell, A. D., Bashford, D., Bellott, M., Dunbrack, R. L., Evanseck, J. D., Field, M. J., … Karplus, M. (1998). All-atom empirical potential for molecular modeling and dynamics studies of proteins. *The Journal of Physical Chemistry. B*, *102*, 3586–3616. https://doi.org/10.1021/jp973084f

Mackerell, A. D. Jr., Feig, M., & Brooks, C. L. 3rd (2004). Extending the treatment of backbone energetics in protein force fields: Limitations of gas-phase quantum mechanics in reproducing protein conformational distributions in molecular dynamics simulations. *Journal of Computational Chemistry*, *25*, 1400–1415. https://doi.org/10.1002/jcc.20065

Mitcheson, J., Perry, M., Stansfeld, P., Sanguinetti, M. C., Witchel, H., & Hancox, J. (2005). Structural determinants for high-affinity block of hERG potassium channels. *Novartis Foundation Symposium*, *266*, 136–150. discussion 150-138

Mitcheson, J. S., Chen, J., Lin, M., Culberson, C., & Sanguinetti, M. C. (2000). A structural basis for drug-induced long QT syndrome. *Proceedings of the National Academy of Sciences of the United States of America*, *97*, 12329–12333. https://doi.org/10.1073/pnas.210244497

Miyake, A., Mochizuki, S., Yokoi, H., Kohda, M., & Furuichi, K. (1999). New ether-a-go-go K^+ channel family members localized in human telencephalon. *The Journal of Biological Chemistry*, *274*, 25018–25025. https://doi.org/10.1074/jbc.274.35.25018

Olsson, M. H., Sondergaard, C. R., Rostkowski, M., & Jensen, J. H. (2011). PROPKA3: Consistent treatment of internal and surface residues in empirical pKa predictions. *Journal of Chemical Theory and Computation*, *7*, 525–537. https://doi.org/10.1021/ct100578z

O'Neil, M. J. (2013). *The Merck index—An encyclopedia of chemicals, drugs, and biologicals*15th edition edn. Cambridge, UK: Royal Society of Chemistry.

Parrinello, M., & Rahman, A. (1981). Polymorphic transitions in single-crystals—A new molecular dynamics method. *Journal of Applied Physics*, *52*, 7182–7190. https://doi.org/10.1063/1.328693

Perrin, M. J., Kuchel, P. W., Campbell, T. J., & Vandenberg, J. I. (2008). Drug binding to the inactivated state is necessary but not sufficient for high-affinity binding to human ether-a-go-go-related gene channels. *Molecular Pharmacology*, *74*, 1443–1452. https://doi.org/10.1124/mol.108.049056

Roden, D. M. (1996). Ionic mechanisms for prolongation of refractoriness and their proarrhythmic and antiarrhythmic correlates. *The American Journal of Cardiology*, *78*, 12–16. https://doi.org/10.1016/S0002-9149(96)00448-1

Saganich, M. J., Machado, E., & Rudy, B. (2001). Differential expression of genes encoding subthreshold-operating voltage-gated K^+ channels in brain. *The Journal of Neuroscience*, *21*, 4609–4624. https://doi.org/10.1523/JNEUROSCI.21-13-04609.2001

Sanchez-Chapula, J. A., Ferrer, T., Navarro-Polanco, R. A., & Sanguinetti, M. C. (2003). Voltage-dependent profile of human ether-a-go-go-related gene channel block is influenced by a single residue in the S6 transmembrane domain. *Molecular Pharmacology*, *63*, 1051–1058. https://doi.org/10.1124/mol.63.5.1051

Sanchez-Chapula, J. A., Navarro-Polanco, R. A., Culberson, C., Chen, J., & Sanguinetti, M. C. (2002). Molecular determinants of voltage-dependent human ether-a-go-go related gene (HERG) K^+ channel block. *The Journal of Biological Chemistry*, *277*, 23587–23595. https://doi.org/10.1074/jbc.M200448200

Sanguinetti, M. C., Jiang, C., Curran, M. E., & Keating, M. T. (1995). A mechanistic link between an inherited and an acquired cardiac arrhythmia: HERG encodes the IKr potassium channel. *Cell*, *81*, 299–307. https://doi.org/10.1016/0092-8674(95)90340-2

Sanguinetti, M. C., & Tristani-Firouzi, M. (2006). hERG potassium channels and cardiac arrhythmia. *Nature*, *440*, 463–469. https://doi.org/10.1038/nature04710

Saxena, P., Zangerl-Plessl, E. M., Linder, T., Windisch, A., Hohaus, A., Timin, E., … Stary-Weinzinger, A. (2016). New potential binding determinant for hERG channel inhibitors. *Scientific Reports*, *6*, 24182. https://doi.org/10.1038/srep24182

Schonherr, R., Gessner, G., Lober, K., & Heinemann, S. H. (2002). Functional distinction of human EAG1 and EAG2 potassium channels. *FEBS Letters*, *514*, 204–208. https://doi.org/10.1016/S0014-5793(02)02365-7

Shi, W., Wang, H. S., Pan, Z., Wymore, R. S., Cohen, I. S., McKinnon, D., & Dixon, J. E. (1998). Cloning of a mammalian elk potassium channel gene and EAG mRNA distribution in rat sympathetic ganglia. *The Journal of Physiology*, *511* (Pt 3), 675–682. https://doi.org/10.1111/j.1469-7793.1998.675bg.x

Tan, P. S., Perry, M. D., Ng, C. A., Vandenberg, J. I., & Hill, A. P. (2012). Voltage-sensing domain mode shift is coupled to the activation gate by the N-terminal tail of hERG channels. *The Journal of General Physiology*, *140*, 293–306. https://doi.org/10.1085/jgp.201110761

Trudeau, M. C., Titus, S. A., Branchaw, J. L., Ganetzky, B., & Robertson, G. A. (1999). Functional analysis of a mouse brain Elk-type K^+ channel. *The Journal of Neuroscience*, *19*, 2906–2918. https://doi.org/10.1523/JNEUROSCI.19-08-02906.1999

Trudeau, M. C., Warmke, J. W., Ganetzky, B., & Robertson, G. A. (1995). HERG, a human inward rectifier in the voltage-gated potassium channel family. *Science*, *269*, 92–95. https://doi.org/10.1126/science.7604285

Vanommeslaeghe, K., Hatcher, E., Acharya, C., Kundu, S., Zhong, S., Shim, J., … Mackerell AD Jr (2010). CHARMM general force field: A force field for drug-like molecules compatible with the CHARMM all-atom additive biological force fields. *Journal of Computational Chemistry*, *31*, 671–690. https://doi.org/10.1002/jcc.21367

Villalba-Galea, C. A., Sandtner, W., Starace, D. M., & Bezanilla, F. (2008). S4-based voltage sensors have three major conformations. *Proceedings of the National Academy of Sciences of the United States of America*, *105*, 17600–17607. https://doi.org/10.1073/pnas.0807387105

Wang, W., & MacKinnon, R. (2017). Cryo-EM structure of the open human ether-a-go-go-related K^+ channel hERG. *Cell*, *169*, 422–430 e410. https://doi.org/10.1016/j.cell.2017.03.048

Webb, B., & Sali, A. (2016). Comparative Protein Structure Modeling Using Modeller. *Current Protocols in Bioinformatics*, *54*, 5.6.1–5.6.37. John Wiley & Sons, Inc.

Wu, W., Gardner, A., & Sanguinetti, M. C. (2015). The link between inactivation and high-affinity block of hERG1 channels. *Molecular Pharmacology*, *87*, 1042–1050. https://doi.org/10.1124/mol.115.098111

Zhang, X., Bertaso, F., Yoo, J. W., Baumgartel, K., Clancy, S. M., Lee, V., … Jegla, T. (2010). Deletion of the potassium channel $K_v12.2$ causes hippocampal hyperexcitability and epilepsy. *Nature Neuroscience*, *13*, 1056–1058. https://doi.org/10.1038/nn.2610

Zou, A., Lin, Z., Humble, M., Creech, C. D., Wagoner, P. K., Krafte, D., … Wickenden, A. D. (2003). Distribution and functional properties of human KCNH8 (Elk1) potassium channels. *American Journal of Physiology. Cell Physiology*, *285*, C1356–C1366. https://doi.org/10.1152/ajpcell.00179.2003

SUPPORTING INFORMATION

Additional supporting information may be found online in the Supporting Information section at the end of the article.

How to cite this article: Dierich M, van Ham WB, Stary-Weinzinger A, Leitner MG. Histidine at position 462 determines the low quinine sensitivity of ether-à-go-go channel superfamily member $K_v12.1$. *Br J Pharmacol*. 2019;176: 2708–2723. https://doi.org/10.1111/bph.14693